

Synthesis, docking study, and in vitro anticancer evaluation of new flufenamic acid derivatives

Ammar I. Al-Bayati¹, Ammar A. Razzak Mahmood², Zainab A. Al-Mazaydeh³,
 Majdoleen S. Rammaha³, Rheda I. Al-bayati⁴, Fatima Alsoubani⁵, Lubna H. Tahtamouni^{3,6}

¹ Department of Pharmaceutical Chemistry, Baghdad College of Medical Sciences, Baghdad, Bab-Al-Mouadam, 10001-Iraq

² Department of Pharmaceutical Chemistry, College of Pharmacy, University of Baghdad, Baghdad, Bab-Al-Mouadam-10001-Iraq

³ Department of Biology and Biotechnology, Faculty of Science, the Hashemite University, Zarqa, Jordan

⁴ Department of Chemistry, College of Science, Al-Mustansiryia University, Baghdad, 10001, Iraq

⁵ Department of Chemistry, Faculty of Science, the Hashemite University, Zarqa, Jordan

⁶ Department of Biochemistry and Molecular Biology, College of Natural Sciences, Colorado State University, Fort Collins, Colorado, USA

Corresponding author: Ammar A. Razzak Mahmood (kubbaammar1963@gmail.com)

Received 1 April 2021 ♦ Accepted 8 May 2021 ♦ Published 21 May 2021

Citation: Al-Bayati AI, Mahmood AAR, Al-Mazaydeh ZA, Rammaha MS, Al-bayati RI, Alsoubani F, Tahtamouni LH (2021) Synthesis, docking study, and in vitro anticancer evaluation of new flufenamic acid derivatives. Pharmacia 68(2): 449–461. <https://doi.org/10.3897/pharmacia.68.e66788>

Abstract

Novel compounds (6–10) were synthesized and confirmed by spectroscopic analysis, including AT-IR, ¹HNMR and CHNS. Their cytotoxic effect was evaluated by MTT assay against two cancer cell lines and two normal cell types. Compound 7 exhibited anticancer activity against MCF-7 breast cancer cell line ($GI_{50} = 63.9 \mu\text{g/ml}$, $148 \mu\text{M}$), without any effect against A549 lung cancer cells, or the normal cells. Compound 7 caused cytotoxicity in MCF-7 breast cancer cells by apoptotic cell death, as suggested by fragmented nuclei after DAPI staining and agarose gel electrophoresis. In addition, treating MCF-7 cells with compound 7 resulted in an increase in the level of caspase 9 mRNA level, and its activation. Moreover, compound 7-treated MCF-7 cells showed enhanced cytochrome c release from the mitochondria to the cytosol, signifying an induction of the intrinsic apoptotic pathway. Finally, compound 7 exhibited epidermal growth factor receptor (EGFR) kinase inhibitory activity at ($EC_{50} = 0.13 \mu\text{M}$), which was matched by molecular docking studies that showed compound 7 might be an important EGFR kinase inhibitor.

Keywords

Apoptosis intrinsic pathway, EGFR binding site, Phenylisothiocyanate, Thiadiazole

Introduction

Cancer, uncontrolled cell growth, is a molecularly heterogeneous disease and a leading cause of death worldwide. According to the American Cancer Society, there is a substantial increase in cancer rates, particularly in African regions (Jemal et al. 2012; Shah et al. 2013). Breast cancer is the most common cancer in women worldwide, accounting for 25% of cancer cases (Shah et al. 2020).

Heterocyclic compounds are of particular interest to medicinal chemists, because of their remarkable chemical and versatile biological profiles. Despite considerable advances in research progress into heterocyclic ring systems, attempts are always being made to find new heterocyclic compounds with versatile bioactivity (Zhou et al. 2020). The 1,3,4-thiadiazole scaffold has attracted special interest due to its inherent and diverse biological response.

The 1,3,4-thiadiazole, a unique structure, is a key motif in heterocyclic chemistry and also has a prominent spot in medicinal chemistry, due to its wide of pharmacological effects (Taha et al. 2017). Importantly, 1,3,4-thiadiazole derivatives were identified for their antibacterial, antifungal, antiviral, anti-inflammatory, anti-anxiety, anti-convulsant, anti-cancer, anti-depressant and anti-tuberculosis activities. Certain drugs containing thiadiazole on the market include acetazolamide, methazolamide, cefazedone, timolol and xanomeline (Hu et al. 2014).

Diverse mechanisms of action are being attributed to the anticancer effects of 1,3,4-thiadiazole moiety, such as inhibiting DNA, RNA, and protein synthesis, inhibiting carbonic anhydrase (Supuran and Scozzafava, 2000), phosphodiesterase-7 (PDE7), histone deacetylase, or acting as an adenosine A3 receptor antagonist. Some thiadiazole derivatives used as HIV protease inhibitors were investigated as potential anti-cancer drugs. These agents are capable of preventing the activation of growth factor receptors and downstream Akt signaling, resulting in endoplasmic reticulum stress, autophagy and cell death (Rajak et al. 2011).

The epidermal growth factor receptor (EGFR) is expressed in 60% of triple negative breast cancers (TNBCs) and triggers disease progression. Efforts to try to inhibit EGFR in unselected TNBC patients had a marginal impact on health outcomes (Maksimovic-Ivanic et al. 2017). Current reviews have also shown that EGFR targeted therapy for breast cancer has some great promise for patients with TNBC, basal-like breast cancer, and inflammatory breast cancer (Harrison et al. 2020). EGFR activation leads to receptor endocytosis with implications for the regulation of downstream signaling effectors, autophagy modulation and cell survival. EGFR is thus, considered to be a promising therapeutic target for breast cancer (Westover et al. 2018).

EGFR-dependent tumors that are initially susceptible to EGFR TKIs (tyrosine kinase inhibitors) may develop threonine mutation of 790 (Mishra et al. 2008). Substitution of this residue in EGFR with bulky methionine may cause resistance by steric interference with TKI binding, including gefitinib and erlotinib. New compounds and drug combinations offer an opportunity to delay or overcome resistance mechanism to EGFR TKIs (Sutter et al. 2006). The present study was carried to design and synthesize new derivatives of 2-(1-(2-fluoro-[1,1-biphenyl]-4-yl)ethyl)-6-(substituted phenyl)imidazole[2,1-b][1,3,4]thiadiazole derived from flufenamic acid, and to assess their antitumor activity *in vitro*, with a kinase inhibition assay, supported by a docking study.

Materials and methods

Experimental part

Flufenamic acid was purchased from Sigma-Aldrich. The infrared spectra were recorded using Shimadzu Specac GS 10800-R IR Affinity-1 Spectrometer ($\nu = \text{cm}^{-1}$). CHNS microanalysis was carried out using a Euro EA3000 elemental analyzer.

^1H NMR spectra of the synthesized compounds were measured on AVANCE-III 400MHz Nanobay FT-NMR spectrometer, using tetramethylsilane (TMS) as an internal standard, the chemical shift was displayed once as (δ , ppm), and $\text{DMSO-}d_6$ was utilized as a solvent.

Chemical synthesis

Synthesis of ethyl 2-((3-(trifluoromethyl)phenyl)amino)benzoate, (Ester) (Mishra et al. 2008)

Flufenamic ethyl ester was prepared in accordance with the method developed by Curtius and Geoble (1888). In a 500 mL round bottom flask with ground glass joint, a mixture of flufenamic acid (0.01 mol, 1.39 g) and 100 mL abs. EtOH was added, and the flask was fitted with a rubber cork carrying an inlet tube as well as a calcium chloride guard tube. Hydrochloric acid dried by bubbling through conc. H_2SO_4 was passed into the mixture till enough gas was dissolved. The flask was fitted with a reflux condenser and the mixture was refluxed. The flufenamic acid completely went into solution within about 30 min. After a total refluxing of 6 h, the flask was allowed to cool, the solution was neutralized with 10% Na_2CO_3 and extracted by four portions of diethyl ether. The ether was evaporated by rotary evaporator and the pure crystals were obtained by recrystallization from 60% EtOH. A colorless flufenamic acid ethyl ester, yield (89%), m.p = 144–146 °C, $R_f = 0.9$, AT-IR ($\nu = \text{cm}^{-1}$): 3313 str of *sec.* (NH_2); 3000–3100 (Ar-CH) str, 2981 str of methyl (CH), 2930 str of methylene (CH), 1685 str of (C = O) conjugated ester carbonyl, 1523,1454, str of Ar (C = C), 1165 (C-O) str of ester 794, 748, 698 str of *ortho* & *meta* substitution.

^1H NMR (500 MHz, $\text{DMSO-}d_6$, δ ppm): 9.36 (s, 1 H, NH) 7.93 (*br d*, $J=7.81$ Hz, 1 H, Ar-H) 7.51–7.56 (m, 5 H Ar-H) 7.32 (*br t*, $J=8.29$ Hz, 1 H, Ar-H) , 6.95 (t, $J=7.62$ Hz, 1 H, Ar-H) ,4.31 (q, 2H, CH_2 *aliph*), 1.31 (t, 3H, CH_3 *aliph*).

Synthesis of 2-((3-(trifluoromethyl)phenyl)amino)benzohydrazide, (hydrazide) (Abbas et al. 2015; Hmood et al. 2021)

Flufenamic ethyl ester, (0.037 mol, 5.6 g) and hydrazine hydrate 99.5% (an excess amount of 0.185 mol, 9.0 mL) were added to 40 mL of EtOH into 250 mL round bottom flask and the mixture was first refluxed at 80 °C for 12 h after which, it was set to be stirred overnight at room temperature (RT). It was noticed that the colorless solution changed into pale pink with the time. At the end, half of the solvent was removed under reduced pressure, and the residue was poured into ice. The precipitate was filtered and washed with ice-cold EtOH to afford a product, afterwards, it was recrystallized from 70% EtOH to yield compound (Hydrazide), yield (80%), m.p = 149–151 °C, $R_f = 0.74$, AT-IR ($\nu = \text{cm}^{-1}$): 3317, 3305 doublets, str of *prim* (NH_2), 3305, 3197 str of *sec* (NH), 1616 bend of (NH), 1523, 1496, 1465 str (Ar C = C) skeleton, 1581 bend of (NH) (amide II band), 1284 str of (C-N), 790, 752, 694 str of *ortho* & *meta* substitutions.

¹H NMR (500 MHz, DMSO-_d₆, δ ppm): 9.85 (*br s*, 1 H, *sec*.NH-amide), 9.52 (*s*, 1 H, NH-amide), 7.61 (*br d*, *J* = 7.81 Hz, 1 H, Ar-H), 7.48 (*br t*, *J* = 7.81 Hz, 1 H, Ar-H), 7.37–7.42 (*m*, 4 H, Ar-H), 7.23 (*br d*, *J* = 7.32 Hz, 1 H, Ar-H), 6.95 (*t*, *J* = 7.32 Hz, 1 H, Ar-H), 4.54 (*br s*, 2 H, NH₂).

General method for synthesis of the compounds (1–5)
(Al-Saad et al. 2019)

To a solution of compound (hydrazide) (0.00364 mol, 0.5 g) in 25 mL of EtOH, the following were added separately [(1): *p*-chloro phenylisothiocyanate (0.00364 mol, 0.78 g), (2): *p*-fluoro phenylisothiocyanate, (0.00364 mol, 0.558g), (3): *p*-bromophenylthiocyanate, (0.00364 mol, 0.558g), (4) phenylisothiocyanate, (0.00364 mol, 0.657 g), and (5): *p*-methylphenylisothiocyanate (0.00364 mol, 0.544g)]. The reaction mixture was stirred at 40–50 °C for 4 h, and then it was kept stirring overnight at RT. Half of the solvent was removed under reduced pressure, and the residue was poured into ice. The precipitate was filtered and washed with ice-cold EtOH, to give a product and re-crystallized from 70% EtOH to yield the corresponding final compounds, (Scheme 1).

N-(4-chlorophenyl)-2-(2-((3-(trifluoromethyl)phenyl)amino)benzoyl)hydrazine-1-carbothioamide (1)

Off-white crystals, yield (94%), m.p = (190–194 °C), *R*_f = 0.89, AT-IR (ν = cm⁻¹): 3363 str of *sec* (NH), 3271 str (NH) of thioamide, 3159 str (NH) of amide, 2962 str of (Ar-CH), 1651 str (C = O) of amide (amide I band), 1581 bend (NH), 1519, 1491, 1446, 1423 str of (Ar C = C) skeleton, 1257 str (C-N), 1211 str (C = S), 829 str *p*-Cl substitution, 794, 740, 698 str *ortho* & *meta* substitutions.

¹H NMR (400 MHz, DMSO-_d₆, δ = ppm): 10.62 (*br s*, 1 H, *sec*.NH-amide), 9.80 (*s*, 1 H, *sec*.NH-amide), 9.60 (*br s*, 1 H, *sec*.NH-thioamide), 7.88 (*br s*, 1 H, Ar-H), 7.31–7.53 (*m*, 9 H Ar-H and *sec*.NH), 7.21 (*br d*, *J* = 7.46 Hz, 1 H, Ar-H), 6.99 (*br t*, *J* = 7.40 Hz, 1 H, Ar-H).

CHNS analysis: Calcd. for (C₂₁H₁₆ClF₃N₄OS) C, 54.25; H, 3.47; N, 12.05; S, 6.90. Observed: C, 54.35; H, 3.69; N, 12.28; S, 6.72.

N-(4-fluorophenyl)-2-(2-((3-(trifluoromethyl)phenyl)amino)benzoyl)hydrazine-1-carbothioamide (2)

White crystals, yield (87.5%), m.p = (104–208 °C), *R*_f = 0.73, AT-IR (ν = cm⁻¹): 3363 str (NH) of *sec*. amide, 3228 str (NH) of thioamide, 3174 str (NH) of amide, 1654 str (C = O) of amide (amide I band), 1604 bend (NH) overlapped with Ar-str of (C = C) skeleton, 1581 bend (NH) of (amide II band), 1504 str of (Ar C = C) skeleton, 1253 str (C-N), 1211 str (C = S), 833 *p*-F substitution, 783, 744, 694 str *ortho* & *meta* substitutions.

¹H NMR (400 MHz, DMSO-_d₆, δ ppm) 10.62 (*br s*, 1 H, *sec*.NH-amide), 9.73 (*br s*, 1 H, *sec*.NH), 7.89 (*br s*, 1 H, Ar-H), 7.41–7.53 (*m*, 7 H, Ar-H, & NH), 7.26 (*br d*, *J* = 7.46 Hz, 1 H, Ar-H), 7.17 (*br t*, *J* = 8.68 Hz, 2 H, Ar-H), 6.99 (*t*, *J* = 7.40 Hz, 1 H, Ar-H).

CHNS analysis: Calcd. for (C₂₁H₁₆F₄N₄OS) C, 56.25; H, 3.60; N, 12.49; S, 7.15. Observed: C, 56.41; H, 3.62; N, 12.36; S, 6.96.

N-(4-bromophenyl)-2-(2-((3(trifluoromethyl)phenyl)amino)benzoyl)hydrazine-1-carbothioamide (3)

White powder, yield (95%), m.p = (180–185 °C), *R*_f = 0.89, FTIR (ν = cm⁻¹): 3356 str of *sec*. amide (NH), 3275 str of thioamide (NH), 3155 str of amide (NH), 1651 str of (C = O) amide (amide I band), 1581 str of (C=N) overlapped with Ar- str of (C = C) of skeleton, 1519 bend of (amide II band) (NH), 1257str (C-N), 1215 str of (C = S), 825 *p*-Br substitution, 794, 740, 698 str *ortho* & *meta* substitutions.

¹H NMR (400 MHz, DMSO-_d₆, δ ppm): 10.62 (*br s*, 1 H, *sec*.NH-amide), 9.81 (*br s*, 1 H, *sec*. NH), 9.61 (*br s*, 1 H, NH-thioamide), 7.88 (*br s*, 1 H, Ar-H), 7.39–7.53 (*m*, 10 H, Ar-H & NH), 7.25 (*br d*, *J* = 7.21 Hz, 1 H, Ar-H), 7.00 (*br t*, *J* = 7.15 Hz, 1 H, Ar-H).

CHNS analysis: Calcd. for (C₂₁H₁₆BrF₃N₄OS) C, 49.52; H, 3.17; N, 11.00; S, 6.30. Observed: C, 49.70; H, 3.01; N, 11.03; S, 6.34.

N-phenyl-2-(2-((3-(trifluoromethyl)phenyl)amino)benzoyl)hydrazine-1-carbothioamide (4)

Off-white powder, yield (90%), m.p = (190–195 °C), *R*_f = 0.63, AT-IR (ν = cm⁻¹): 3371 str of *sec*. amide (NH), 3228 str of thioamide (NH), 3163 str of amide (NH), 1651 str of (C = O), amide (amide I band), 1597 str of (C=N) overlapped with Ar-str vibrations of (C=C) skeleton, 1527 bend of (amide II band) (NH), 1257str (C-N), 1215 str (C = S), 786, 740, 692 str *ortho* & *meta* substitutions.

¹H NMR (400 MHz, DMSO-_d₆, δ ppm): 10.62 (*br s*, 1 H, *sec*.NH-amide), 9.82 (*br s*, 1 H, *sec*.NH), 9.59 (*br s*, 1 H, NH-thioamide), 7.80 (*br s*, 1 H, Ar-H), 7.46–7.66 (*m*, 6 H, Ar-H & NH), 7.31–7.41 (*m*, 4 H, Ar-H), 7.27 (*br d*, *J* = 7.46 Hz, 1 H, Ar-H), 7.17 (*m*, 1 H, Ar-H) 7.00 (*br t*, *J* = 7.34 Hz, 1 H, Ar-H).

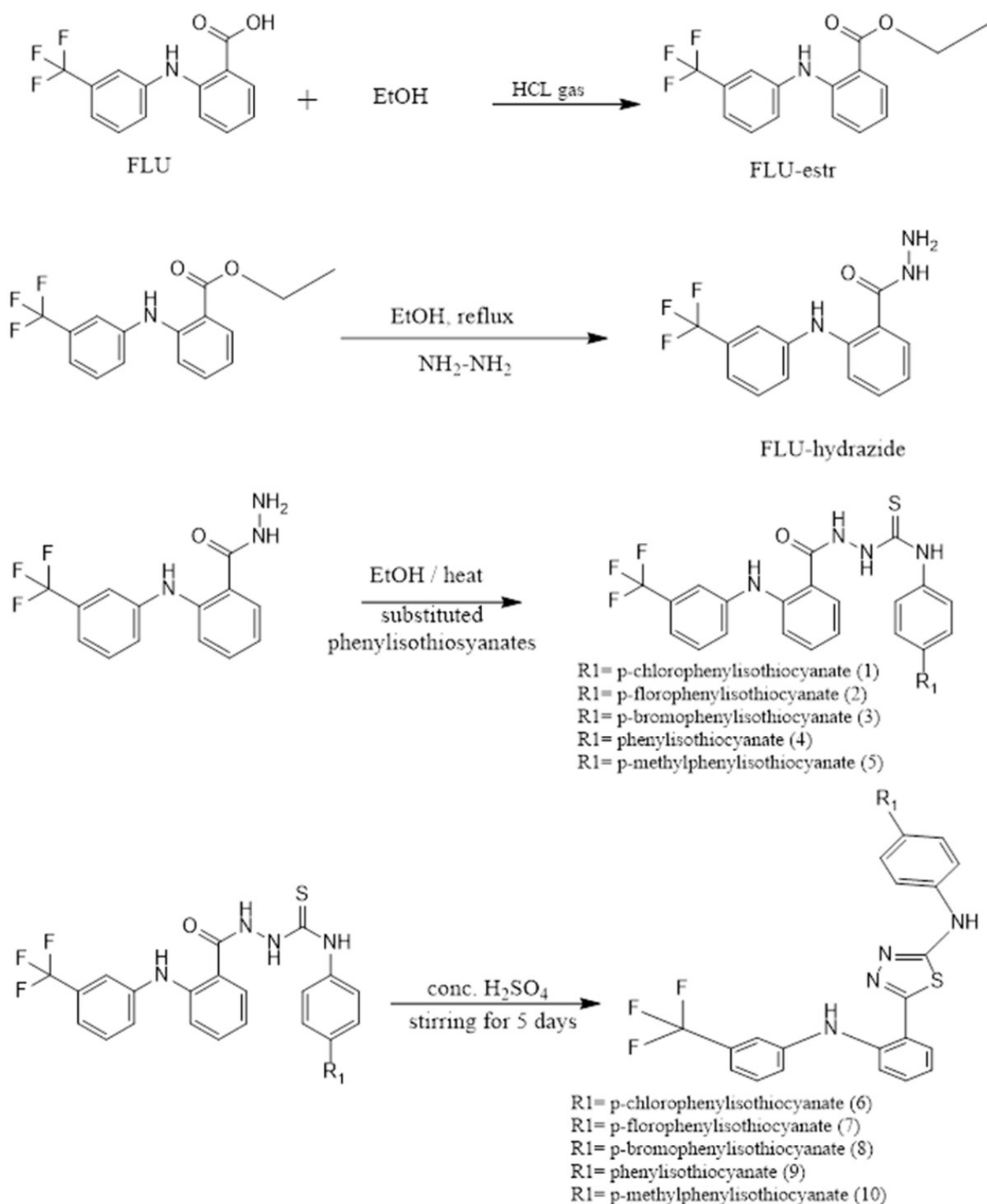
CHNS analysis: Calcd. for (C₂₁H₁₇F₃N₄OS) C, 58.60; H, 3.98; N, 13.02; S, 7.45. Observed: C, 58.80; H, 4.20; N, 13.23; S, 7.23.

N-(*p*-tolyl)-2-(2-((3-(trifluoromethyl)phenyl)amino)benzoyl)hydrazine-1-carbothioamide (5)

White powder, yield (92%), m.p = (189–192 °C), *R*_f = 0.64, ATIR (ν = cm⁻¹): 3360 str of *sec*. amide (NH), 3267 str of thioamide (NH), 3228 str of amide (NH), 3140 str of Ar-(CH), 1651 str of (C = O) amide (amide I band), 1581 str of (C=N) overlapped with aromatic -stretching of (C = C) skeleton, 1519 bend of (amide II band) (NH), 1330 (CH) *sym* in-plane bend of (–CH₃), 1257 str (C-N), 1215 str (C = S), 817 *p*-CH₃-substitution, 794, 740, 663 *ortho* & *meta* substitutions.

¹H NMR (400 MHz, DMSO-_d₆, δ ppm) 10.59 (*br s*, 1 H, *sec*.NH-amide), 9.75 (*br s*, 1 H, *sec*.NH), 9.62 (*br s*, 1 H, NH-thioamide), 7.87 (*br s*, 1 H, Ar-H), 7.42–7.53 (*m*, 6 H, Ar-H & NH), 7.21–7.40 (*m*, 3 H, Ar-H), 7.14 (*br d*, *J* = 7.83 Hz, 2 H, Ar-H), 6.99 (*br t*, *J* = 7.34 Hz, 1 H, Ar-H), 2.29 (*s*, 3 H, CH₃, *aliph*).

CHNS analysis: Calcd. for (C₂₂H₁₉F₃N₄OS) C, 59.45; H, 4.31; N, 12.61; S, 7.21. Observed: C, 59.61; H, 4.31; N, 12.67; S, 7.15.



Scheme 1. Scheme representing synthesis of the titled compounds (1-10).

General method for synthesis of the compounds (6-10) (Szeliga and Monika 2020)

Hydrazinecarbothioamide compounds (1-5) (0.001 mol) were added separately to 5 mL conc. H_2SO_4 at 0 °C, and stirred for 3 h at RT. It was noticed that a clear yellow solution appeared. The reaction mixture was neutralized with 2N NaOH and filtered, afterwards, it was washed with a

plenty amount of H_2O . The precipitate was recrystallized with 70% EtOH to afford the titled compounds (6-10).

N-(4-chlorophenyl)-5-(2-((3-(trifluoromethyl)phenyl)amino)phenyl)-1,3,4-thiadiazol-2-amine (6)

Pale brown powder, yield (42%), m.p = (75-77 °C), $R_f = 0.52$, ATIR ($\nu = \text{cm}^{-1}$): 3259,3194 str of sec. amine (NH), 3043str of Ar (CH), 1616,1600,1581,1562 bend of

(NH), and str (C = N), 1492, 1516 str of Ar-(C = C), 1219 str (C-N), 624 str (C-S-C), 821 str *p*-Cl-substitution, 794, 729, 694 *ortho* & *meta* substitutions.

¹H NMR (400 MHz, DMSO-_{d6}, δ = ppm): 10.57 (s, 1 H, *sec.* NH-TDZ), 9.12 (s, 1 H, NH), 7.98 (dd, *J* = 7.82, 1.10 Hz, 1 H, Ar-H), 7.69–7.72 (m, 2 H, Ar-H), 7.38–7.43 (m, 6 H, Ar-H), 7.18–7.24 (m, 3 H, Ar-H).

CHNS analysis: Calcd. for (C₂₁H₁₄ClF₃N₄S) C, 56.44; H, 3.16; N, 12.54; S, 7.18. Observed: C, 56.66; H, 3.32; N, 12.71; S, 7.26.

N-(4-fluorophenyl)-5-(2-((3-(trifluoromethyl)phenyl)amino)phenyl)-1,3,4-thiadiazol-2-amine (7)

Pale brown powder, yield (30%), m.p (83–86 °C), *R_f* = 0.30, ATIR (ν = cm⁻¹): 3259,3217 str of *sec.* amine (NH), 2997 str of Ar(CH), 1624, 1581 bend of (NH) and str (C = N), 1485,1423 str of Ar-(C = C), 1226 str (C-N), 613 str (C-S-C), 821 *p*-F- substitution, 750, 729, 698 *ortho* & *meta* substitutions.

¹H NMR (400 MHz, DMSO-_{d6}, δ = ppm) 10.46 (s, 1 H, *sec.* NH TDZ), 9.13 (s, 1 H, NH), 7.97 (d, *J* = 7.46 Hz, 1 H, Ar-H), 7.68–7.70 (m, 2 H, Ar-H), 7.46–7.52 (m, 3 H, Ar-H), 7.17–7.24 (m, 6 H, Ar-H).

CHNS analysis: Calcd. for (C₂₁H₁₄F₄N₄S) C, 58.60; H, 3.28; N, 13.02; S, 7.45. Observed: C, 58.81; H, 3.48; N, 13.24; S, 7.63.

N-(4-bromophenyl)-5-(2-((3-(trifluoromethyl)phenyl)amino)phenyl)-1,3,4-thiadiazol-2-amine (8)

Brown powder, yield (35%), m.p = (88–92 °C), *R_f* = 0.9, FTIR (ν = cm⁻¹): 3278,3190 str of *sec.* amine (NH), 3035 str of Ar-(C-H), 1612,1597,1562 bend of (NH), and str (C = N), 1492,1527,1423 str of Ar-(C = C), 1219 str (C-N), 613 str (C-S-C), 817 *p*-Br substitution, 794, 744,732,698 *ortho* & *meta* substitutions.

¹H NMR (400 MHz, DMSO-_{d6}, δ = ppm): 10.58 (s, 1 H, NH-TDZ), 9.11 (s, 1 H, *sec.* NH), 7.98 (d, *J* = 7.83 Hz, 1 H, Ar-H), 7.65 (d, *J* = 8.93 Hz, 2 H, Ar-H), 7.43–7.53 (m, 5 H, Ar-H), 7.19–7.23 (m, 4H, Ar-H). CHNS analysis: Calcd. for (C₂₁H₁₄BrF₃N₄S) C, 51.34; H, 2.87; N, 11.40; S, 6.53. Observed: C, 51.23; H, 3.10; N, 11.61; S, 6.47.

N-phenyl-5-(2-((3-(trifluoromethyl)phenyl)amino)phenyl)-1,3,4-thiadiazol-2-amine (9)

Pale brown powder, yield (50%), m.p = (90–93 °C), *R_f* = 0.74, ATIR (ν = cm⁻¹): 3263,3190 str of *sec.* amine (NH), 3055,3028 str of Ar-(CH), 1597,1566 bend of (NH) and str (C = N), 1496,1539,1445,1419 str of Ar-(C = C), 1226 str (C-N), 632 str (C-S-C), 790,752,729,664 *ortho* & *meta* str substitutions.

¹H NMR (400 MHz, DMSO-_{d6}, δ = ppm): 10.44 (s, 1 H, *sec.* NH), 9.15 (s, 1 H, NH-TDZ), 7.97 (d, *J* = 7.57 Hz, 1 H, Ar-H), 7.66 (d, *J* = 7.82 Hz, 2 H, Ar-H), 7.35–7.46 (m, 5 H, Ar-H), 7.19–7.25 (m, 4 H, Ar-H), 7.01 (t, *J* = 7.34 Hz, 1 H, Ar-H).

CHNS analysis: Calcd. for (C₂₁H₁₅F₃N₄S) C, 61.16; H, 3.67; N, 13.58; S, 7.77. Observed: C, 58.25; H, 4.05; N, 12.92; S, 8.71.

N-(*p*-tolyl)-5-(2-((3-(trifluoromethyl)phenyl)amino)phenyl)-1,3,4-thiadiazol-2-amine (10)

Brown powder, yield (46%), m.p (92–96 °C), *R_f* = 0.89, FTIR (ν = cm⁻¹): 3248,3186 str of *sec.* amine (NH), 3116,3032 str of Ar-(CH), 1616,1597,1570,1535 bend of (NH) and str (C = N), 1535,1516,1469,1450,1423 str of Ar-(C = C), 1219 str (C-N), 617 str (C-S-C), 817 *p*-methyl substitution, 790,748,729,694 *ortho* & *meta* substitutions.

¹H NMR (400 MHz, DMSO-_{d6}, δ = ppm) 10.34 (s, 1 H, NH-TDZ), 9.17 (s, 1 H, *sec.* NH), 7.94 (d, *J* = 7.54 Hz, 1 H, Ar-H), 7.54 (d, *J* = 8.31 Hz, 2 H, Ar-H), 7.38–7.50 (m, 3 H, Ar-H), 7.12–7.28 (m, 6 H, Ar-H), 2.26 (s, 3H, *aliph.* CH₃).

CHNS analysis: Calcd. for (C₂₂H₁₇F₃N₄S) C, 61.96; H, 4.02; N, 13.14; S, 7.52. Observed: C, 30.48; H, 2.22; N, 6.58; S, 7.14.

Biological analysis

Cell culture

Human A549 lung cancer cell line was cultured in Ham's F-12K (Kaighn's) medium (Gibco, USA) supplemented with 10% fetal bovine serum (FBS; Capricorn Scientific, Germany), human MCF-7 breast cancer cells were cultured in RPMI-1640 medium (Euroclone, Italy) supplemented with 10% FBS, The mammary non-tumorigenic MCF10A cell line was grown in DMEM/F12 (Gibco, USA) supplemented with 5% horse serum (Invitrogen, USA), EGF (20 ng/mL, Sigma), hydrocortisone (0.5 mg/mL, Sigma), cholera toxin (100 ng/mL, Sigma) and insulin (10 µg/mL, Sigma) and white blood cells (WBC) were cultured in RPMI-1640, supplemented with 5% FBS. Trypsin-EDTA (Lonza, Switzerland) was used throughout for subcultures. Cell growth was attained at 37 °C in 5% carbon dioxide and 95% air.

In vitro cytotoxicity (3-(4,5-dimethylthiazol-2-yl)-2,5-diphenyltetrazolium bromide) MTT assay

The cytotoxicity of the parent compounds (1–5) and the various 1,3,4-thiadiazole derivatives (6–10) against different cell lines (A549, MCF-7 and MCF10A), and WBC was evaluated using an MTT assay (tetrazolium salt reduction) assay (Bacanli et al. 2017; Han et al. 2018). Drug stock solutions were prepared at 10% DMSO; the final concentration of DMSO in the media did not exceed 0.1%. Seven concentrations (0.5, 1, 2.5, 5, 10, 25 and 50 µg/ml) were prepared for each compound in the growth media. Viable cells (50,000) were added to each well of a 96-well tissue culture plate containing a growth medium complemented by FBS. Cells were kept in a humidified 5% CO₂ incubator at 37 °C for 24 h. The next morning, the different concentrations were added, and the cells incubated for 24 h, 48 h, and 72 h. Freshly prepared MTT salt (3-(4,5-dimethylthiazol-2-yl)-2,5-diphenyltetrazolium bromide; Sigma) (5 mg/mL) was then added to each well to afford a final concentration of 0.5 µg/µl. The plates were incubated for 4 h, and the formation of formazan

crystals was checked using an inverted microscope. Equal volume of 1:1 (200 μ l) DMSO and isopropanol mixture was added to each well, and incubated for 30–45 min. The inhibition of cell growth induced by the vitamins was detected by measuring the absorbance of each well at 570 nm using a Biotek Synergy HT Multi-Mode Microplate Reader (VT, USA). Percent growth was calculated according to the following formula: Growth (%) = OD treated/OD vehicle-treated control \times 100%. The concentration-percent growth curve was used to compute the required concentration that caused 50% growth inhibition (GI_{50}) by linear interpolation from a semi-log plot of a dose response curve. The test was repeated three times in triplicates.

Detection of apoptosis

Apoptosis was identified by microscopic analysis of apoptotic nuclei upon DAPI staining (Jabir et al. 2021a). Cells were plated on sterile glass cover slips for 24 h. Cells were subsequently treated with different prepared compounds at the GI_{50} concentration. Samples were treated with 4% paraformaldehyde (Sigma, USA) in phosphate buffered saline (PBS) for 45 min. The cells were then washed with PBS 3 times 3 min each. Cells were then mounted with Prolong Gold Antifade containing DAPI (Invitrogen). Images were captured using a 100 \times NA 1.3 objective on a Nikon Eclipse Ti-E microscope with a CCD camera and operated by NIS-Elements software. In addition, DNA fragmentation was evaluated by electrophoresis on agarose gel (Jabir et al. 2020). Briefly, DNA from control, and treated cells was extracted according to the manufacturer's instructions (Wizard Genomic DNA Purification, Promega). DNA samples were electrophoresed on a 1.5% agarose gel containing 5 μ l/100 mL of RedSafe nucleic acid staining solution (iNtRON Biotechnology, South Korea). The gel was analyzed and photographed by using ultraviolet gel documentation system (FluorChem R System, Oxford, UK).

Quantitative reverse transcription-polymerase chain reaction (qRT-PCR)

The quantity of caspase 4, caspase 8, caspase 9 mRNA was assessed by qRT-PCR (Tahtamouni et al. 2018; Nawasreh et al. 2020). Total RNA from vehicle-treated control and GI_{50} -treated cells was extracted as per the manufacturer instructions (Total RNA Isolation System, Sigma-Aldrich, USA). After the extraction of RNA, cDNA was prepared using the power cDNA synthesis kit (iNtRON Biotechnology, South Korea). Amplification of target cDNA for apoptosis markers and β -actin (as a normalization gene) was done using KAPA SYBR FAST qPCR Kit Master Mix (KAPA BIOSYSTEMS, USA) on Line Gene 9680 BioGR instrument. cDNA (5 μ l aliquots) was mixed with 1 μ l of forward primer (25X), 1 μ l reverse primer (25X) (Kondo et al. 2009; Yaoxian et al. 2015). 5.5 μ l nuclease free water and 12.5 μ l master mixture. All experiments were performed in triplicate. The relative amount of caspases mRNA was normalized to β -actin mRNA.

Western blot analysis

Control and GI_{50} -treated cells were washed 3 times with cold PBS, and then lysed with protein lysis buffer [10%

sodium dodecyl sulfate (SDS), 1 M Tris buffer pH 7.5, 1 M sodium fluoride (NaF), 1M dithiothreitol (DTT), 0.1 M ethylene glycol tetraacetic acid (EGTA), and D.W on ice. The cell lysate was collected and boiled for 5 min and sonicated. Aliquots of lysates were diluted in 4x SDS-PAGE sample buffer (0.5 M Tris-HCl pH 6.8, 2% SDS, 20% glycerol, 20% 2-mercaptoethanol and 0.16% bromophenol blue), and proteins were resolved by electrophoresis on 10% or 12.5% SDS-polyacrylamide gels. Proteins were transferred onto nitrocellulose membranes and were blocked using 2% (w/v) BSA in Tris-buffered saline (TBS), and subjected overnight at 4°C to the primary antibodies: rabbit polyclonal anti-caspase 4 (1:1000; Invitrogen, USA), mouse monoclonal anti-caspase 8 (1:1000; Invitrogen, USA), mouse monoclonal anti-caspase 9 (1:1000; Invitrogen, USA), mouse monoclonal anti-GAPDH (1:6000; CHEMICON, USA), rabbit polyclonal anti-tubulin (1:3000; abcam, USA), diluted in 1% BSA in TBS containing 0.05% Tween 20. After washing and incubation with appropriate secondary antibodies conjugated to IRDye 680 or 800 nm fluorescent dyes, the membranes were washed, and the bands were analyzed on FluorChem R system (Oxford, UK). Signals were validated using AlphaView software (ProteinSimple, USA) (Jabir et al. 2021b).

Cytochrome c release apoptosis assay

5 \times 10⁷ control and GI_{50} -treated cells were recovered by centrifugation at 2,900 RPM for 5 min, washed with ice cold PBS, and centrifuged at 2,900 RPM for 5 min, and re-suspended with 1X cytosolic extraction buffer mix containing dithiothreitol (DTT), and protease inhibitors. The cells were incubated on ice for 10 min, homogenized and centrifuged at 3,100 RPM for 10 min. The supernatant was centrifuged again at 12,000 RMP for 30 min to obtain the cytosolic fraction, while the pellet was re-suspended in mitochondrial extraction buffer to collect the mitochondrial fraction (Cytochrome c Release Apoptosis Assay Kit, Abcam, USA).

EGFR kinase inhibitory assay

The *in vitro* inhibitory activity of the synthesized compound(s) against EGFR was accomplished using EGFR(T790M/L858R) Kinase Assay Kit (BPS Bioscience, USA). Briefly, EGFR and its substrate were incubated with the synthesized compounds in enzymatic buffer for 40 min at 30 °C to launch the enzymatic reaction. The reaction was terminated by addition of detection reagent (Kinase-Glo Max reagent, Promega), followed by incubation at RT for 15 min. The remaining activity of EGFR kinase was observed by measuring chemiluminescence using a Biotek Synergy HT Multi-Mode Microplate Reader (VT, USA). The concentration-percent remaining EGFR kinase activity curve was also used to calculate the concentration that caused 50% kinase activity inhibition (the effective concentration that inhibits 50% of EGFR kinase activity; EC_{50}). All samples and controls were verified in duplicate.

Statistical analysis

All experiments were performed in duplicates or triplicates. The results were presented as average \pm SEM.

Statistical analysis was carried out using GraphPad Prism version 5.0. (GraphPad Software, San Diego, CA, USA). The Student's t-test was also used to test for significant differences in means. The p value <0.05 was considered to be significant (Al Rugaie et al. 2021).

Molecular docking study

In terms of choosing molecular targets, the newly synthesized compounds (6–10) may function on, and try comparing them with other ligands, and to determine the pharmacophoric functionality that may enable binding to the critical amino acid(s) at the target site, the target site was chosen by the protein data bank (<https://www.rcsb.org/>). Target compounds are tested in practice against many active sites, and the outcomes will then determine the proper protein for molecular docking. Upon selecting a particular protein, some operations were carried out, and provide insight into the molecular binding modes of the tested compounds within the pocket of the epidermal growth factor receptor tyrosine kinase (ATP binding site of EGFR kinase), using the MOE 2015 software. The binding sites were generated from co-crystallized ligand in crystal protein (PDB codes: 1ywn) (Al-Saad et al. 2019). Initially, the water molecules would be removed from the complex, accompanied by the correction of crystallographic disorders and unfilled valence atoms using protein report, and utility and clean protein options. The use of CHARMM and MMFF94 force fields was carried out to minimize protein energy. The rigid binding site was the protein structure obtained by applying a fixed atom constraint. The protein essential amino acids were defined and prepared for the docking process. The 2D structures of the tested compounds were drawn using Chem-Bio Draw Ultra14.0, and saved in MDL-SD file format from MOE 2015 software, the saved file was opened, the 3D structures were protonated, and the energy was kept to a minimum by applying 0.05 RMSD CHARMM force field. The minimized structures were again prepared for docking employing ligand preparation protocol (Szeliga and Monika 2020).

Results and discussion

Biological activity

Cytotoxicity of the target derivatives is cancer-cell specific

The cytotoxicity of the five parent compounds (1–5) and the five different thiadiazole derivatives (6–10) was investigated against two human cancer cell lines (A549 and MCF-7), and two normal cell types (MCF10A and WBC) by the *in vitro* cytotoxicity MTT assay. The corresponding GI_{50} (50% Growth Inhibition) values for each compound against cancer cells are shown in Table 1. The findings suggest that none of the compounds were effective against the A549 lung carcinoma cells; 20% maxi-

Table 1. The MTT assay results, the values shown are GI_{50} .

Compound	A549	MCF-7
1	No effect ^b (20%)*	No effect ^b (16%)*
2	No effect ^b (17%)*	No effect ^b (40%)*
3	No effect ^b (0%)*	No effect ^b (27%)*
4	No effect ^b (16%)*	No effect ^b (28%)*
5	No effect ^b (0%)*	No effect ^b (8%)*
6	No effect ^b (15%)*	75.2 µg/mL (169.1 µM) ^a
7	No effect ^b (11%)*	63.9 µg/mL (148 µM) ^a
8	No effect ^b (11%)*	No effect ^b (25%)*
9	No effect ^b (4%)*	No effect ^b (14%)*
10	No effect ^b (0%)*	24.7 µg/mL (57.92 µM) ^a

*: Maximum growth inhibition after 72 h of treatment with the highest concentration a: 48 h, b: 72 h.

mum growth inhibition upon 72 h of treatment with the highest concentration (50 µg/mL). However, three of the thiadiazole compounds (6, 7 and 10) exhibited cytotoxic effects against MCF-7 breast cancer cells (Table 1, Figure 1A). The lack of cytotoxicity of any of the thiadiazole compounds against A549 lung cancer cells was not surprising, different types of cancer cells vary in their response to chemotherapeutic drugs (Niepel et al. 2017). Cytotoxic effects against A549 cells could have been achieved if higher concentrations of these drugs were used (higher than 50 µg/mL). Another explanation could be that these derivatives work against A549 lung cancer cells in a mechanism that was not investigated in the current work, such as cell adhesion, polarization or migration, the current work focused on cell proliferation induced mainly by EGFR signaling, however, our future plans are to pursue other signaling pathways that might be affected by these derivatives in A549 lung cancer cells such as actin cytoskeleton dynamics and cell migration (Tahtamouni et al. 2013). Although compound 10 was the most potent (lowest GI_{50} value after 48 h of treatment), it showed chemo-resistance at 72 h, thus compound 7 which exhibited consistent cytotoxic effects within the testing period (72 h), was chosen to pursue the other biological assays. Unless otherwise stated, the amount of compound 7 used in subsequent experiments was the GI_{50} value from this table. Likewise, the data suggest that the compound 7 did not cause more than 10% growth inhibition in the two normal cells tested (MCF-10A and WBC; Fig. 1B), reflecting that the compound is a cancer-cell. specific.

Cytotoxicity of compound 7 is attributed to induction of apoptosis

The results presented in Fig. 2 showed that compound 7 caused cytotoxicity in MCF-7 breast cancer cells by induction of apoptosis, as indicated by fragmented nuclei after DAPI staining (Fig. 2A) and agarose gel electrophoresis (Fig. 2B). Treating MCF-7 breast cancer cells with DMSO at 0.5% or 1% did not trigger apoptosis (Fig. 2A). On the other hand, nuclei of cells treated with 5% DMSO for 48 h were smaller in size than control cells, and few were fragmented (Fig. 2A). However, DNA extracted from 5% DMSO treated cells did not produce fragmentation (Fig. 2B).

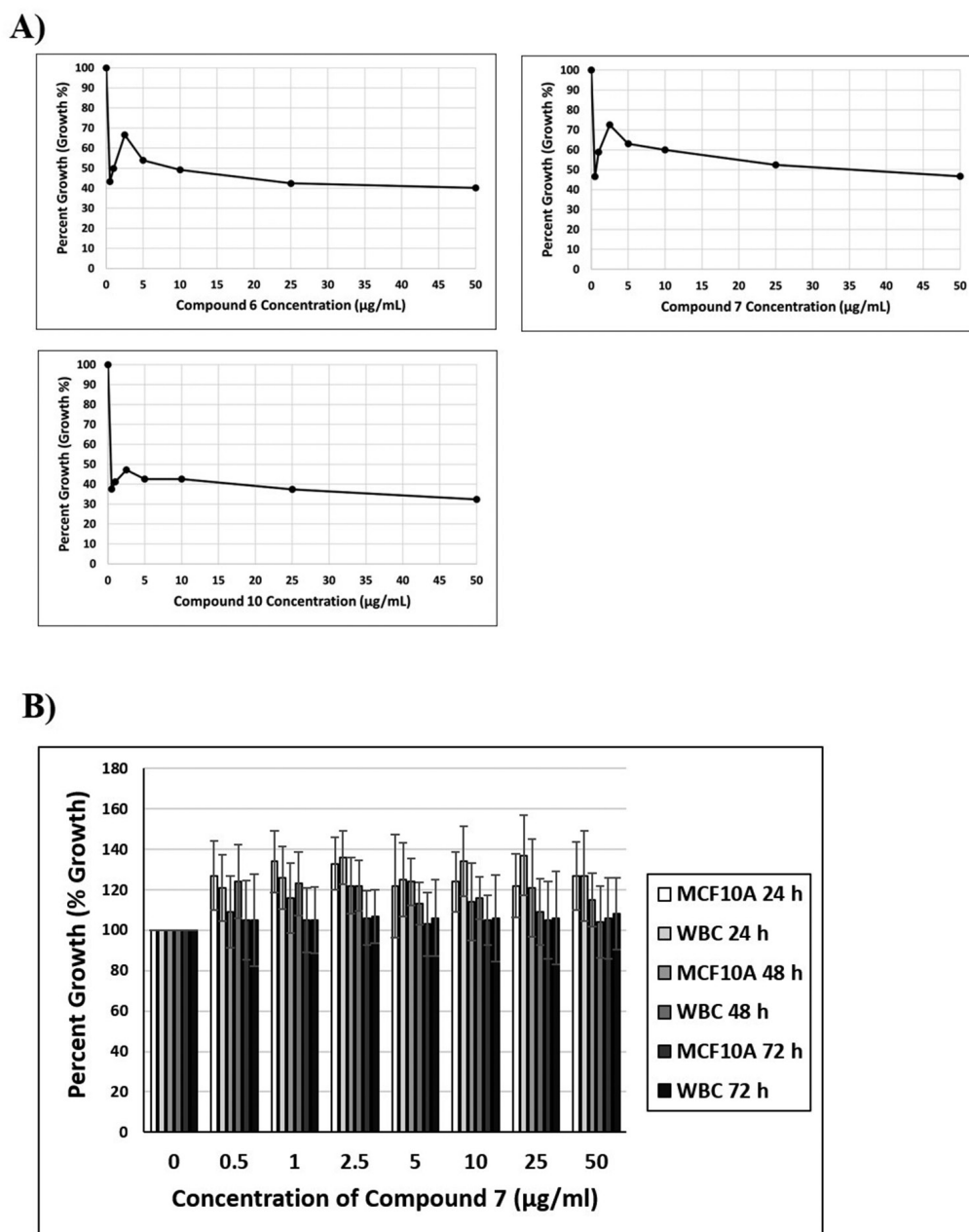


Figure 1. The MTT assay results for A) The cytotoxic compounds (6, 7 and 10) after 48 h of treatment, B) Compound 7 against non-tumorigenic MCF10A cells and WBC.

Compound 7 induction of apoptosis is dependent on activation of caspase 9

In order to investigate the role of caspase activation downstream of compound 7 induction of apoptosis, the mRNA levels of caspase 4, caspase 8 and caspase 9 were tested by qRT-PCR (Fig. 3A), and their activation (cleavage) was validated by western blotting (Fig. 3B). Treatment of MCF-7 breast cancer cells with 0.5% or 1% DMSO did not lead to an increase in the mRNA levels of any of the caspases compared to the vehicle-treated control cells (Fig. 3A) or their activation (cleavage) (Fig. 3B). On the other hand, the treatment of these cells with 5% DMSO or compound 7 led to a significant increase in caspase 9 mRNA level (Fig. 3A) and its activation (Fig. 3B). None of the treat-

ments affected caspase 4 or 8 mRNA levels or caused their activation (Fig. 3). Additionally, treating MCF-7 breast cancer cells with compound 7, but not 5% DMSO caused the release of cytochrome c from the mitochondria to the cytosol, as compared to control cells (Fig. 3C).

Compound 7 exhibit EGFR kinase inhibitory activity

Compound 7 was tested for its EGFR kinase inhibitory activity using a commercial EGFR Kinase Assay Kit. 5% DMSO was used as a negative control (Fig. 4). Compound 7 showed comparable inhibitory activity (0.13 µM) to what was published for erlotinib (a potent epidermal growth factor receptor (EGFR) inhibitor, 0.387 12 µM (Sutter et al. 2006).

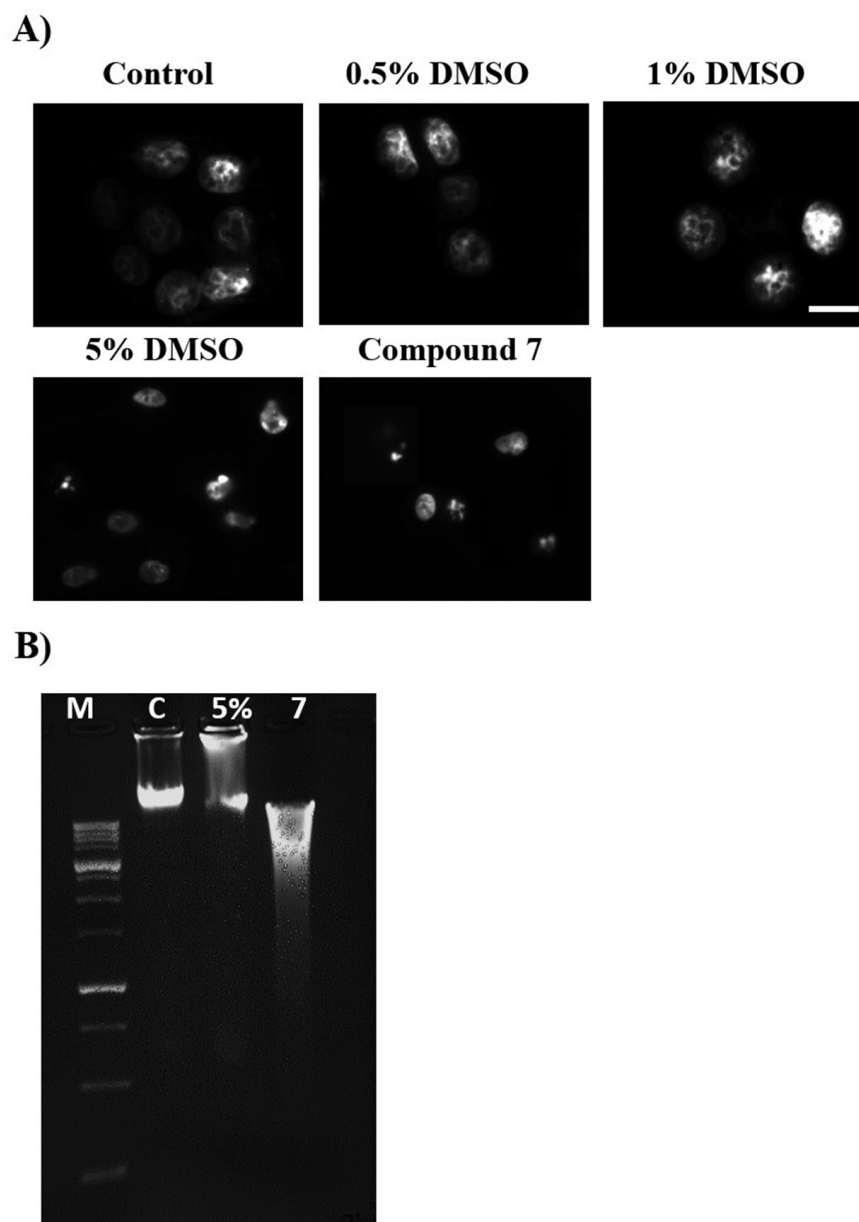


Figure 2. Compound 7 induces apoptosis in MCF-7 breast cancer cells. **A)** Fluorescence images of MCF-7 breast cancer cells showing fragmented nuclei after DAPI staining. Scale bar: 10 μ m, **B)** Detection of DNA fragmentation by agarose gel electrophoresis. Cells were treated and genomic DNA was extracted and electrophoresed on 1.5% agarose gels. M: DNA molecular weight marker; C: vehicle-treated control cells; 5%: 5% DMSO-treated cells; 7: Compound 7-treated cells. Three experiments were performed with similar results.

Molecular docking processes

Molecular docking process was carried out using CDOCKER protocol. CDOCKER is a grid-based molecular docking methodology that employs CHARMM-based molecular dynamics (MD) system to dock the ligands into a binding pocket. The receptor was held rigid while the ligands were allowed to be flexible during the refining process. The docking score (CDOCKER interaction energy) of the best fitting poses with the active site, the ATP binding site of EGFR kinase was recorded (Table 2). This was used to estimate the proposed binding mode, affinity, preferred orientation of each docking pose, and

Table 2. Show (ΔG) kcal/mol of tested candidates against (EGFR) target site PDB ID: 1ywn.

Comp. NO.	Interactions		Score (ΔG) kcal/mol	RMSD Value/ $^{\circ}$ A
	H.B	<i>pi</i>		
1	3	0	-6.84	1.97
2	4	0	-6.82	1.95
3	3	0	-6.40	1.74
4	3	0	-6.68	1.59
5	1	0	-6.99	1.48
6	2	1	-8.12	1.27
7	2	1	-7.79	1.22
8	2	1	-8.12	1.39
9	2	1	-7.70	1.29
10	1	1	-7.31	1.56
Erlotinib	0	3	-6.36	1.68

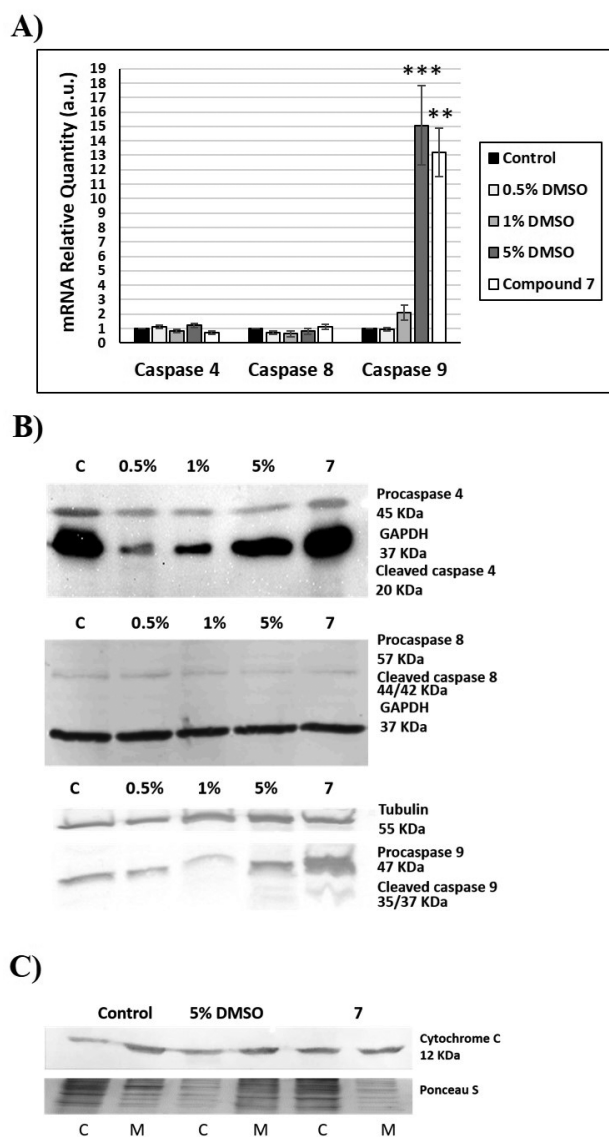


Figure 3. Compound-7 induced apoptosis is dependent on caspase 9 activation and cytochrome c release. A) qRT-PCR analysis of caspase 4, 8 and 9 mRNA in compound 7-treated cells (GI_{50}) as compared to vehicle-treated control cells [set as 1 arbitrary unit (a.u.)]. Values were normalized to β -actin. Bars = mean \pm SEM. of three independent experiments performed in triplicates. * $P < 0.05$ compared to vehicle-treated control cells, B) Representative Western blots showing cleavage “activation” of procaspase 9 to the active forms p35/p37, C) Representative Western blot showing the release of cytochrome c from the mitochondria (M) into the cytosol (C) of treated MCF-7 breast cancer cells (GI_{50}). Equal protein loading was controlled by staining membranes with Ponceau S (a representative section of the stained membrane is shown). The experiment was repeated three times.

binding of the free energy of the tested compounds to the ATP binding site of EGFR kinase. The measured interaction energies for the compounds tested were in total consistent with the observed result, which showed that compound 7 might have potent inhibitory activity against EGFR kinase. Each molecule was allowed to produce seven different interaction poses with the protein. The key of binding site consists of amino acids Asp776,

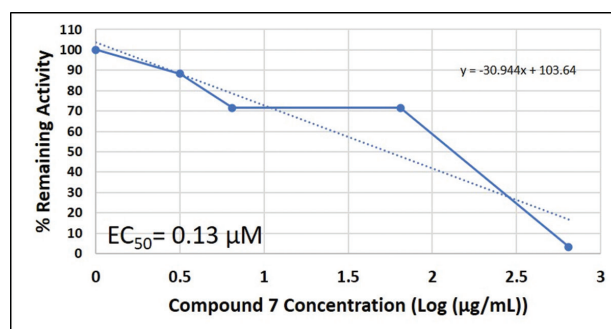


Figure 4. *In vitro* EGFR kinase enzymatic inhibitory activity of compound 7. EC_{50} = the effective concentration that inhibits 50% of EGFR kinase activity.

Thr766, leu694, Cys773, Gly772 and Val702 for EGFR tyrosine kinase (Patel et al. 2018).

The binding mode of compound 6 exhibited an energy binding of -8.12 kcal/mol. The 1,3,4-thiadiazole ring formed a hydrogen bonding with Lys721 at a distance of 2.12 Å, as well as, the *p*-chloro phenyl group formed one hydrogen bonding with Met742, at a distance of 3.17 Å. The hydrophobic phenyl moiety formed one *pi*-interaction with Val702 (Fig. 5A). The binding mode of compound 7 exhibited an energy binding of -7.79 kcal/mol. The 1,3,4-thiadiazole ring formed H-bond with Lys721 at a distance of 2.58 Å.

Meanwhile, tri-fluoro phenyl group formed a new *pi*-interaction with Asp831, and hydrophobic phenyl moiety formed one *pi*-interaction with Val702 (Fig. 5B). Compound 8 had a binding energy of -8.12 kcal/mol. The 1,3,4-thiadiazole ring formed H-bond with Lys721 at a distance of 2.71 Å, and the *p*-bromo phenyl group formed a single H-bond with Met742 at a distance of 3.44 Å, while the hydrophobic phenyl moiety formed one *pi*-interaction with Val702 (Fig. 5C). Compound 9 produced an energy binding of -7.70 kcal/mol. The NH bridge established H-bond with Asp831, at a distance of 1.91 Å, while the hydrophobic tri-fluoro phenyl moiety formed two *pi*-interactions with Leu694 and Cys773 (Fig. 5D). Finally, the binding mode of compound 10 exhibited an energy binding of -7.31 kcal/mol. The 1,3,4-thiadiazole ring formed H-bond with Asp831 at a distance of 3.41 Å, and the hydrophobic tri-fluoro phenyl moiety formed one *pi*-interaction with Leu694 (Fig. 5E).

***In-silico* ADMET, and carcinogenicity analysis**

Absorption, distribution, metabolism, excretion, and toxicity (ADMET) prediction was carried out with the ADMET descriptor module of the small molecules protocol of the pre ADMET online software.

The partition coefficient (Clogp) values of the target compounds are greater than > 5 , and they still follow the Lipinski rule of five, that states the number of hydrogen bond donors (HBD), and hydrogen bond acceptors (HBA) are within the Lipinski's limit range (Beg et al. 2020). Whereas the Clogs for these compounds ranges from -7.48 to -6.45 , this implies poor solubility of the synthesized derivatives in water. As a general principle, if the bioactivity score is large, there is a high possibi-

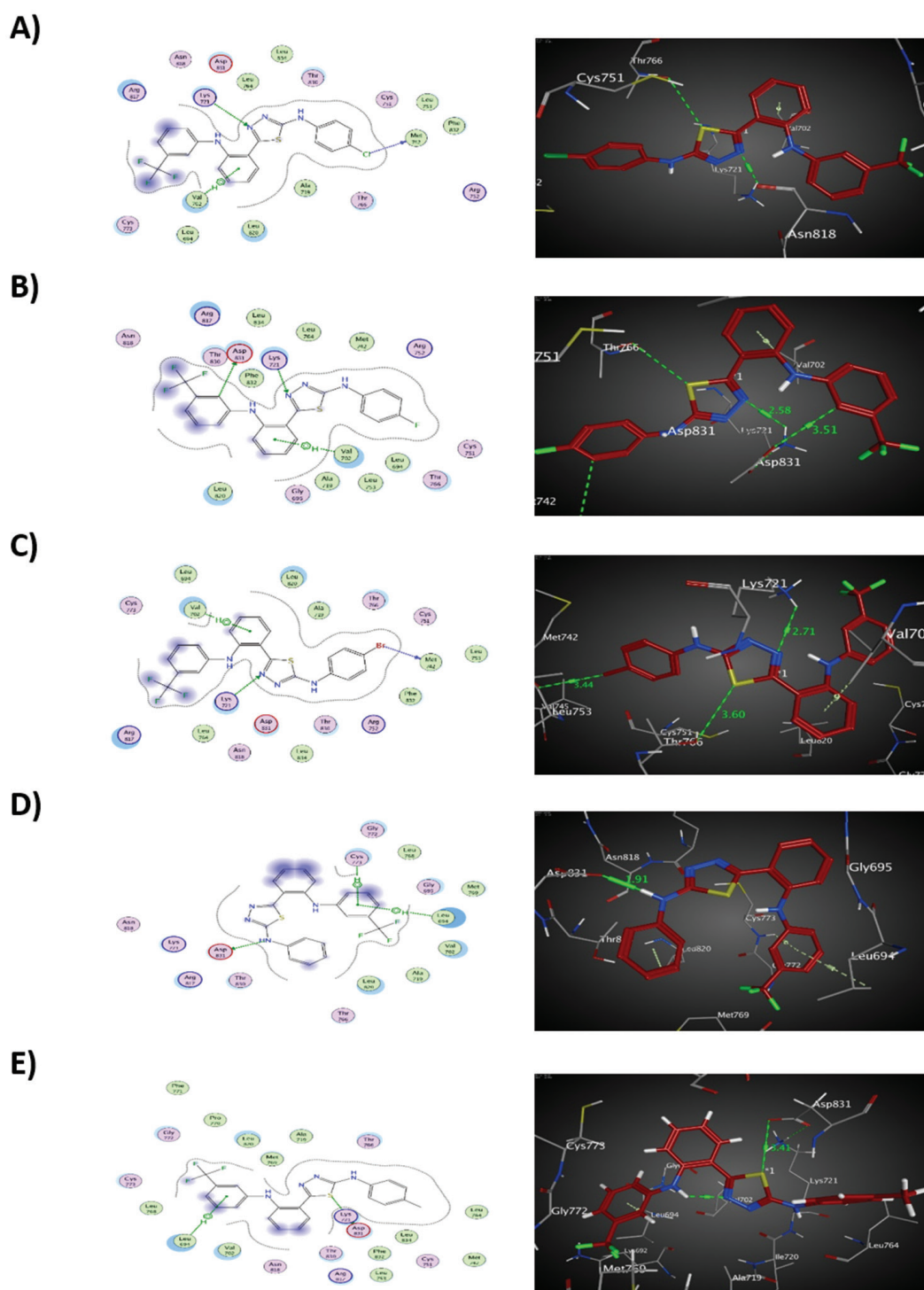


Figure 5. 2D and 3D view of the target compounds (6-10) docked in ATP binding site of EGFR kinase [A) Compound 6, B) compound 7, C) compound 8, D) compound 9, E) compound 10].

ty that the compound under investigation will be active. Therefore, a compound having bioactivity score of more than 0.00 is most likely to have a significant biological activity, while values between -0.50 to 0.00 are expected to be moderately active, and if the score is less than -0.50 it is presumed to be inactive (Ezekiel A et al. 2017). As for the log K_p for the skin permeability, which reflects the transport of the molecules through the epidermis, the more negative the log K_p , the less the skin permeates the

molecule (Bonzanini and Lopes 2014; Gaur et al. 2015; Rudrapal et al. 2017).

The extent of absorption of GIT molecules appears to be low, yet, these derivatives possess low penetration to the blood brain barrier (BBB), and would have no effect on CNS activity. Finally, the data generated in (Table 3) showed that none of the compounds are mutagenic nor carcinogenic, suggesting that the hit compounds are expected to be safe (Patel et al. 2018).

Table 3. The ADMET properties of the titled compounds (1-10).

Properties	Comp1	Comp 2	Comp3	Comp 4	Comp 5	Comp 6	Comp 7	Comp 8	Comp 9	Comp 10
M.wt	464.89	448.44	509.34	430.45	444.47	446.88	430.42	491.33	412.43	426.46
c log p < 5	5.36	5.09	5.55	4.88	5.03	6.15	5.88	6.24	5.60	5.9
c log s	-7.04	-6.61	-7.36	-6.45	-6.75	-7.17	-6.73	-7.48	-6.58	-6.87
nHBA ≤10	4	5	4	4	4	5	6	5	5	5
nHBD ≤5	4	4	4	4	4	2	2	2	2	2
nrtb	9	9	9	9	9	6	6	6	6	6
n. violation	1	1	2	1	1	1	1	1	1	1
B.A score	0.55	0.55	0.17	0.55	0.55	0.55	0.55	0.55	0.55	0.55
(log Kp) cm/s	-4.08	-4.35	-4.30	-4.31	-4.14/	-4.08	-4.36	-4.31	-4.32	-4.15
G.I. absorption	low									
Mutagenic	None									
Tumorigenic	None									
Irritant	None									
LL score	3	3	3	3	3	2	2	2	2	2
TPSA ≤ 140 °A	97.28	97.28	97.28	97.28	97.28	78.06	78.08	78.08	78.08	78.08
BBB	NO									

Notes: Clog p= calculated logarithm of partition coefficient between *n*-octanol and water, Clog s= calculate logarithm of solubility, nHBA= Number of hydrogen bond acceptor, nHBD= Number of hydrogen bond donor, n rtb. = Number of rotatable bonds, n.violation= Number of violations for Lipinski Rule of five, violations are (logP>4.15, MW>500). B.A. score= Bioactivity score of the synthesized compounds (1-10), Log Kp= Log of skin permeation, LL score= Lead likeness model score, compounds having zero or negative values should not be considered as a drug-like candidates, violations are (MW>350, log p>3.5, Rotors>7). TPSA= Topological polar surface area, BBB= Blood brain barrier,

Conclusions

Novel thiadiazole compounds (6–10) were synthesized from the parent flufenamic acid, and confirmed by spectroscopic analysis, including AT-IR, ¹HNMR and CHNS. Their cytotoxic activity against two human cancer cell lines (A549 and MCF-7), and the non-tumorigenic MCF10A and WBC was evaluated by the MTT assay. Three of the five derivatives (compounds 6, 7 and 10) showed significant cell growth inhibition against MCF-7 cell line. Compound 7 exhibited the lowest and more consistent anticancer activity against MCF-7 cell line (GI₅₀ = 63.9 µg/mL), with no effect on A549 cell line or normal cells.

Compound 7 caused cytotoxicity against MCF-7 breast cancer cells by induction of apoptosis, as indicated by fragmented nuclei after DAPI staining, and agarose gel electrophoresis. Moreover, compound 7 led to an in-

crease in caspase 9 mRNA level and its activation. Also, compound 7-treated MCF-7 cells showed enhanced cytochrome c release from the mitochondria to the cytosol, indicating an induction of the intrinsic apoptotic pathway. Finally, compound 7 showed EGFR kinase inhibitory activity (EC₅₀ = 0.13 µM), which was matched by the molecular docking studies, that showed compound 7 may be considered as plausible inhibitor of EGFR kinase. This study could serve as a basis for optimizing other derivatives for better interaction with EGFR kinase enzyme.

Acknowledgements

We thank the Department of Pharmaceutical Chemistry, College of Pharmacy, University of Baghdad for their support, and work facilities in the laboratory.

References

- Abbas A, Amer N, Fadhil AA (2015) Synthesis, characterization and biological evaluation of new potentially active hydrazones of naproxen hydrazide. *Der Pharma Chemica* 7(10): 93–101.
- Al Rugaie O, Jabir M, Kadhim R, Karsh E, Sulaiman G, Mohammed S, Mohammed H (2021) Gold nanoparticles and graphene oxide flakes synergistic partaking in cytosolic bactericidal augmentation: role of ROS and NOX2 ctivity. *Microorganisms* 9(1): e101. <https://doi.org/10.3390/microorganisms9010101>
- Al-Saad N, Mahmood A, Al-Bayati R (2019) Design, synthesis, docking study and antiplatelet evaluation of new thiosemicarbazide derivatives derived from captopril. *Oriental Journal of Chemistry* 35(2): 829–838. <https://doi.org/10.13005/ojc/350246>
- Bacanli M, Hatice G, Başaran A, Nurşen B (2017) Fenoliklerin sitotoksitesisite profillerinin değerlendirilmesi: Farklı hücrelerde farklı zaman aralıklarında nötral kırmızı ve MTT yöntemlerinin karşılaştırılması. *Turkish Journal of Pharmaceutical Sciences* 14(2): 95–107. <https://doi.org/10.4274/tjps.07078>
- Beg M, Athar F (2020) Pharmacokinetic and molecular docking studies of *Achyranthes Aspera* phytocompounds to exploring potential antituberculosis activity. *Journal of Bacteriology and Mycology* 8(1): 18–27. <https://doi.org/10.15406/jbmoa.2020.08.00268>
- Bonzanini R, Lopes A (2014) Inibição de ciclooxigenases 1 (COX-1) e 2 (COX-2) por monoterpenos: Um estudo in silico cyclooxygenase 1 (COX-1) and 2 (COX-2) inhibition by monoterpenes: An in silico study. *UNOPAR Cient Ciênc Biol Saúde* 16(4): 307–316.
- Ezekiel A, Odumosu P, Ojerinde S (2017) Synthesis, drug likeness and antioxidant activity of analogues of l-Arginine. *Organic and Medicinal Chemistry International Journal* 1(5): 1–4.
- Gaur R, Thakur J, Yadav D, Kapkoti D, Verma R, Gupta N, Saikia D, Bhakuni R (2015) Synthesis, antitubercular activity, and molecular modeling studies of analogues of isoliquiritigenin and liquiritigenin, bioactive components from *Glycyrrhiza Glabra*. *Medicinal Chemistry Research* 24(9): 3494–3503. <https://doi.org/10.1007/s00044-015-1401-1>
- Han D, Wu X, Liu L, Shu W, Huang Z (2018) Sodium tanshinone IIA sulfonate protects ARPE-19 cells against oxidative stress by inhibiting autophagy and apoptosis. *Scientific Reports* 8(1): 1–15. <https://doi.org/10.1038/s41598-018-33552-2>

- Harrison P, Vyse S, Huang P (2020) Rare epidermal growth factor receptor (EGFR) mutations in non-small cell lung cancer. *Seminars in Cancer Biology* 61(1): 167–179. <https://doi.org/10.1016/j.semcancer.2019.09.015>
- Hmood K, Mahmood A, Al-bayati R, Abdulrahman S (2021) Synthesis, docking study and *in vitro* antitumor evaluation of some new flurbiprofen derivatives against MCF-7 and WRL-68 cell lines. *Indonesian Journal of Pharmacy* 32(1): 17–34. <https://doi.org/10.22146/ijp.730>
- Hu L, Wang X, Yong-Hua Y, Hai-Liang Zh (2014) 1,3,4-Thiadiazole: Synthesis, reactions, and applications in medicinal, agricultural, and materials chemistry. *Chemical Reviews* 114(10): 5572–5610. <https://doi.org/10.1021/cr400131u>
- Jabir M, Sahib U, Taqi Z, Taha A, Sulaiman G, Albukhaty S, Rizwana H (2020) Linalool-loaded glutathione-modified gold nanoparticles conjugated with CALNN peptide as apoptosis inducer and NF- κ B translocation inhibitor in SKOV-3 cell line. *International Journal of Nanomedicine* 15: e9025. <https://doi.org/10.2147/IJN.S276714>
- Jabir M, Hussien A, Sulaiman G, Yaseen N, Dewir Y, Alwahibi M, Rizwana H (2021a) Green synthesis of silver nanoparticles from *Eriobotrya japonica* extract: a promising approach against cancer cells proliferation, inflammation, allergic disorders and phagocytosis induction. *Artificial Cells, Nanomedicine, and Biotechnology* 49(1): 48–60. <https://doi.org/10.1080/21691401.2020.1867152>
- Jabir M, Saleh Y, Sulaiman G, Yaseen N, Sahib U, Dewir Y, Soliman D (2021b) Green Synthesis of silver nanoparticles using *Annona muricata* extract as an inducer of apoptosis in cancer cells and inhibitor for NLRP3 inflammasome via enhanced autophagy. *Nanomaterials* 11(2): e384. <https://doi.org/10.3390/nano11020384>
- Jemal A, Bray F, Forman D, O'Brien M, Ferlay J, Center M, Parkin M (2012) Cancer burden in Africa and opportunities for prevention. *Cancer* 118(18): 4372–4384. <https://doi.org/10.1002/cncr.27410>
- Kondo T, Oka T, Sato H, Shinou Y, Washio K, Takano M, Morito T, Takata K, Ohara N, Ouchida M, Shimizu K, Yoshino T (2009) Accumulation of aberrant CpG hypermethylation by *Helicobacter pylori* infection promotes development. *International Journal of Oncology* 35(1): 547–557. https://doi.org/10.3892/ijo_00000366
- Maksimovic-Ivanic D, Fagone P, McCubrey J, Bendtzen K, Mijatovic S, Nicoletti F (2017) HIV-protease inhibitors for the treatment of cancer: repositioning HIV protease inhibitors while developing more potent NO-hybridized derivatives?. *International Journal of Cancer* 140(8): 1713–1726. <https://doi.org/10.1002/ijc.30529>
- Ashutosh M, Veerasamy R, Jain PK, Dixit VK, Agrawal RK (2008) Synthesis, characterization and pharmacological evaluation of amide prodrugs of flurbiprofen. *Journal of the Brazilian Chemical Society* 19(1): 89–100. <https://doi.org/10.1590/S0103-50532008000100014>
- Ritsuko N, Nakamura T, Mori Y, Takeuchi K (2017) Microwave-assisted facile and rapid esterification of amino acids I: Esterification of l-leucine from batch to flow processes and scale-Up. *Natural Science* 09(04): 110–122. <https://doi.org/10.4236/ns.2017.94011>
- Nawasreh M, Alzyoud E, Al-Mazaydeh Z, Rammaha M, Yasin S, Tahtamouni L (2020) Biological activity and apoptotic signaling pathway of C11-functionalized cephalostatin 1 analogues. *Steroids* 158(1): 108–118. <https://doi.org/10.1016/j.steroids.2020.108602>
- Niepel M, Hafner M, Duan Q, Wang Z, Evan O, Chung M (2017) Common and cell-type specific responses to anti-cancer drugs revealed by high throughput transcript profiling. *Nature Communications*. 1186(8) 24–35. <https://doi.org/10.1038/s41467-017-01383-w>
- Patel N, Moksha N (2018) Targeting epidermal growth factor receptors inhibition in non-small-cell lung cancer: A computational approach. *Molecular Simulation* 44(17): 1478–1488. <https://doi.org/10.1080/0892702.2.2018.1515484>
- Patel H, Kiran D, Yogesh S, Sanjay S, Rajshekhkar K, Neeta T, Mahamadhanif S, Malleshappa N, Rakesh J (2018) In search of selective 11 β -HSD type 1 inhibitors without nephrotoxicity: an approach to resolve the metabolic syndrome by virtual based screening. *Arabian Journal of Chemistry* 11(2): 221–231. <https://doi.org/10.1016/j.arabjc.2015.08.003>
- Rajak H, Avantika A, Poonam P, Bhupendra S, Ravichandran V, Prabodh C, Murli D (2011) 2,5-Disubstituted-1,3,4-oxadiazoles/thiadiazole as surface recognition moiety: Design and synthesis of novel hydroxamic acid based histone deacetylase inhibitors. *Bioorganic and Medicinal Chemistry Letters* 21(19): 5735–5738. <https://doi.org/10.1016/j.bmcl.2011.08.022>
- Rudrapal M, Chetia D, Singh V (2017) Novel series of 1,2,4-trioxane derivatives as antimalarial agents. *Journal of Enzyme Inhibition and Medicinal Chemistry* 32(1): 1159–1173. <https://doi.org/10.1080/14756366.2017.1363742>
- Shah A, Metzger O, Bartlett C, Liu Y, Huang Y, Cristofanilli M (2020) Hormone receptor-positive/human epidermal growth receptor 2-negative metastatic breast cancer in young women: Emerging data in the era of molecularly targeted agents. *The Oncologist* 25(6): 900–908. <https://doi.org/10.1634/theoncologist.2019-0729>
- Shah U, Shah R, Acharya S, Acharya N (2013) Novel anticancer agents from plant sources. *Chinese Journal of Natural Medicines* 11(1): 16–23. [https://doi.org/10.1016/S1875-5364\(13\)60002-3](https://doi.org/10.1016/S1875-5364(13)60002-3)
- Supuran C, Scozzafava A (2000) Carbonic anhydrase inhibitors - part 94. 1,3,4-thiadiazole-2-sulfonamide derivatives as antitumor agents? *European Journal of Medicinal Chemistry* 35(1): 867–874. [https://doi.org/10.1016/S0223-5234\(00\)00169-0](https://doi.org/10.1016/S0223-5234(00)00169-0)
- Sutter A, Höpfner M, Huether A, Maaser K, Scherübl H (2006) Targeting the epidermal growth factor receptor by erlotinib (Tarceva) for the treatment of esophageal cancer. *International Journal of Cancer* 118(7): 1814–22. <https://doi.org/10.1002/ijc.21512>
- Szeliga M (2020) Thiadiazole derivatives as anticancer agents. *Pharmacological Reports* 72(5): 1079–1100. <https://doi.org/10.1007/s43440-020-00154-7>
- Taha M, Javid M, Imran S, Selvaraj M (2017) Synthesis and study of the α -amylase inhibitory potential of thiadiazole quinoline derivatives. *Bioorganic Chemistry* 74(1): 179–186. <https://doi.org/10.1016/j.bioorg.2017.08.003>
- Tahtamouni L, Shaw A, Hasan M, Yasin S, Bamburg J (2013) Non-overlapping activities of ADF and cofilin-1 during the migration of metastatic breast tumor cells. *BMC Cell Biology* 14(45): 1471–2121. <https://doi.org/10.1186/1471-2121-14-45>
- Tahtamouni L, Nawasreh M, Al-Mazaydeh Z, Al-Khateeb R, Abdellatif R, Bawadi R, Bamburg J, Yasin S (2018) Cephalostatin 1 analogues activate apoptosis via the endoplasmic reticulum stress signaling pathway. *European Journal of Pharmacology* 818(8): 400–409. <https://doi.org/10.1016/j.ejphar.2017.11.025>
- Westover D, Cho B, Lovly C, Paz-Ares L (2018) Mechanisms of acquired resistance to first- and second-generation EGFR tyrosine kinase inhibitors. *Annals of Oncology* 29(Supplement 1): i10–19. <https://doi.org/10.1093/annonc/mdx703>
- Yaoxian W (2015) Emodin induces apoptosis of human cervical cancer Hela c via intrinsic mitochondrial an extrinsic death receptor path. *Cancer Cell International* 71(13): 1–8. <https://doi.org/10.1186/1475-2867-13-71>
- Zhou L, Qu R, Yang G (2020) An overview of spirooxindole as a promising scaffold for novel drug discovery. *Expert Opinion on Drug Discovery* 15(5): 603–625. <https://doi.org/10.1080/17460441.2020.1733526>